

Bayesian Calibration for Activity Based Models

Laura Schultz, Joshua Auld and Vadim Sokolov*

First Draft: December, 2019
This Draft: March 8, 2022

Abstract

We consider the problem of calibration and uncertainty analysis for activity-based transportation simulators. ABMs rely on statistical models of traveler’s behavior to predict travel patterns in a metropolitan area. Input parameters are typically estimated from traveler’s surveys using maximum likelihood. We develop an approach that uses Gaussian process emulator to calibrate an activity-based model of a metropolitan transplantation system. Our approach extends traditional emulators to handle high-dimensional and non-stationary nature of the transportation simulator. Our methodology is applied to transportation simulator of Bloomington, Illinois. We calibrate key parameters of the model and compare to the ad-hoc calibration process.

1 Introduction

Activity-based simulators represent each traveler’s activity patterns and trips throughout the day through choice models. The generated trips are then simulated in the traffic flow simulator. These behaviorally-realistic models, require high-resolution representation of network flows and thus, are computationally expensive. This paper focuses on calibrating the choice model parameters used in activity-based simulators. The goal of calibration is to find values of simulator’s input parameters that minimize the deviance between observed and simulated traffic flows. The relation between the observed traffic flows y and the output of the simulator $\eta(z, \theta)$ is given by

$$y(z) = \eta(z, \theta) + \epsilon(\theta) + e, \quad (1)$$

where η is the simulator with observed inputs z we are certain about (e.g. day of the week) and θ represents the inputs we are not certain about (e.g. value of traveler’s time) and need to estimate; $\epsilon(\theta)$ captures structural inadequacy of the simulator; and e is the observation error and the residual variation inherent to the true process that generates y .

The very same flexibility that makes simulation models appealing, also comes hand in hand with calibration problems that are intractable, with the number of simulations required to find an optimal solution growing exponentially, as the input dimension increases [88]. As a result, the use of simulators is currently limited to what-if analysis. Because of the complexity of transportation simulators, straightforward application of existing optimization techniques have limited applicability [34]. There are two major challenges inhibiting the development of efficient optimization algorithms: (i) the non-linear, non-stationary, and stochastic nature of the transportation simulators, and (ii) computational cost of running the simulator. This proposal addresses mentioned challenges by linking advances in probability and machine learning with specifics of transportation simulators to address challenging optimization problems. To support adoption of optimization algorithms, open research and educational content are designed to improve computational and decision making under uncertainty skills within several engineering disciplines. Specifically, there are two research and one educational objective:

The problem of simulator calibration is well studied in the transportation literature [7]. While formal optimization methods [104, 103] are applicable for some types of transportation simulators, the unavailability of derivatives for ABM simulators make calibration efforts computationally demanding [69].

*Vadim Sokolov is Assistant Professor in Operations Research at George Mason University. email:vsokolov@gmu.edu

Simulation-based optimization problems were considered in the literature and typically rely on black-box approaches [95, 66, 8, 108], such as Genetic Algorithm (GA) [21, 61, 65], Simultaneous Perturbation Stochastic Approximation (SPSA) [60, 23, 56], and exhaustive evaluation [44] with relative success [102].

However, research has primarily focused on the traditional, aggregated models which used origin-destination estimation to represent demand [18, 106, 105].

however, in addition to the evaluation limitations of costly evaluation run times, when faced with the high-dimensional inputs, these algorithms require an exponential number of simulator runs (curse of dimensionality) and quickly become impractical.

Modern approaches for research and planning purposes heavily rely on, and have standardized, the behavioral realism captured by high-dimensional activity-based models but alternative calibration approaches to address dimensional shortcomings are not well studied. Current practical approaches remain ad-hoc.

One alternative is to substitute lower fidelity simulators to approximate the solution [22, 74]. However, while this multi-fidelity approach does improve the problem of costly run times, the volume of evaluations to combat the curse of dimensionality issue remains unaddressed. Real-life high fidelity transportation simulators take several hours to days per run [3] but, in the unlikely case that the run-time of a 20-dimensional simulator were to be successfully reduced to only 1 second, 3.171 trillion years of computing time will still be required to evaluate just 10 points per dimension (10^{20} runs). Further, development of these lower-fidelity models would be necessary and results in significantly increased modeling efforts and resources, e.g. modeler's effort and budgets.

Another, approach to solve the problem of calibration relies on the non-parametric Gaussian Process (GP) technique. It was originally developed for uncertainty analysis of computer simulations by [80] and expanded by Kennedy and O'Hagan [52] for calibration purposes.

By combining a probabilistic distribution known as a Gaussian Process(GP) and Bayesian inference, practitioners combated limited sampling through the construction of a cheaper, probabilistic surrogate which could approximate input-output relations [41, 93, 28, 75, 77] through efficient sampling [15, 37, 74, 41, 47, 96, 91, 92, 78].

able to provide a confidence value and analytic capability not necessarily produced by other general-purpose approaches.

However, while providing the necessary flexibility, non-parametric approaches have continued to prove inadequate [89, 31] when faced with the additional complications of high input dimensionality and sensitivity routinely encountered in transportation simulations. Specifically, non-linearities in the simulator violates the smoothness assumption used to reduce sampling size and requires GP approximators to require larger sample sizes to obtain accuracy in high dimensions.

Although Bayesian techniques have been successfully applied to calibration within the transportation field [45, 36, 35, 107] through variable subsetting [71] and pre-processing techniques like Principal Component Analysis [30]. The Gaussian Process based approaches were not thoroughly studied for this application [85, 86].

While vast literature exists on modeling non-stationary and non-homogeneous relations [41, 84, 13, 83]. However, the curse of dimensionality problem continues to be unsolved [89]. Modeling, uncertainty analysis, and optimization applications have, as a result, historically been restricted to characteristically low-dimensional problems [90, 24, 10, 14, 53, 94, 97]. Illustratively, evaluating only the corner points of a 10-dimensional simulation taking 1 second to run will require $2^{10} = 17.1$ minutes to complete; however, evaluating just 10 points per dimension quickly escalates to $10^{10} = 517.1$ years.

Approaches that address the problem of dimensionality include increases in and parallelization of computing resources [39, 104, 100, 25, 29, 87, 98], hierarchical decomposition to sub-problems [16, 67], and stark simplifications to the model [8]; however, even these methods retain some dimensional limitations.

Another set of approaches that address dimensionality issue rely on dimensionality reduction and exploit model structure [33, 32, 51, 62, 70, 12, 24, 6]. Dimensionality Reduction seeks influential substructures to obtain a low dimensional input that is a projection of the original high-dimensional one. Dimensionality Reduction techniques [2, 40] include variable screening [63, 20, 81, 72], kernel construction [58, 26, 99, 32, 48], Partial Least Squares (PLS), Principal Component Analysis (PCA), and sliced inverse regression (SIR).

An alternative approach proposed in this paper relies on nonlinear dimensionality reduction techniques and Bayesian optimization [80].

We solve the problem of non-stationarity and high dimensionality by pre-processing the inputs θ by finding a non-linear map $\phi(\cdot)$ so that the relation between $\phi(\theta)$ and \mathcal{L} can be modeled by a traditional GP approximate. The goal for the map ϕ is to reduce the dimensional relationship and to make the input-output relation stationary so that a classical GP approximator can be used.

Our approach relies on nonlinear DR techniques to empower previously ineffective nonlinear regression methods. More specifically, we use deep learning, non-linear dimension reducer. Our Bayesian optimization algorithm solves the problem of Equation (5) by sequentially constructing an approximation f to the loss function $\mathcal{L}(\phi(\theta))$. We start by putting a prior on continuous functions $C[0, \infty]$ and at each iteration of the algorithm, we choose a new point $\theta^{(*)}$ evaluate the loss function $\mathcal{L}(\theta^*)$ and then we compute a posterior (integrate).

This paper's contributions include:

- Formulation of a Gaussian Process Bayesian surrogates for transportation optimization
- Adaptation of non-linear dimensionality reduction techniques for complexity control
- Development of a framework under which our model can be compared with other similar approaches

The rest of the paper is organized as follows: in Section 2, we detail the typical structure of transportation simulators and the paper's example agent-based model POLARIS [3]; Section 3.1 provides exploratory analysis of the simulator to motivate our methodology. Section 3 outlines the methodological contribution of this paper; Section 4 demonstrates our methodology on the problem of calibrating our example model; and Section 5 discusses avenues for future research.

2 POLARIS: an Agent-Based Model

An activity-based transportation simulator has two components: network and demand. The demand simulator includes several inputs, such as land use variables, socio-demographic characteristics of the population, road infrastructure, and congestion patterns. Then the activity-based models generate the trip tables. Parameters of statistical models that generate the trips are typically estimated using small-sample surveys. Inadequacy of the models combined with low sample sizes lead to structural errors and large unexplained variance in those models. The network component uses trips generated by the demand model as an input and calculates the resulting congestion patterns. Figure 1 shows an example of the the overall architecture.

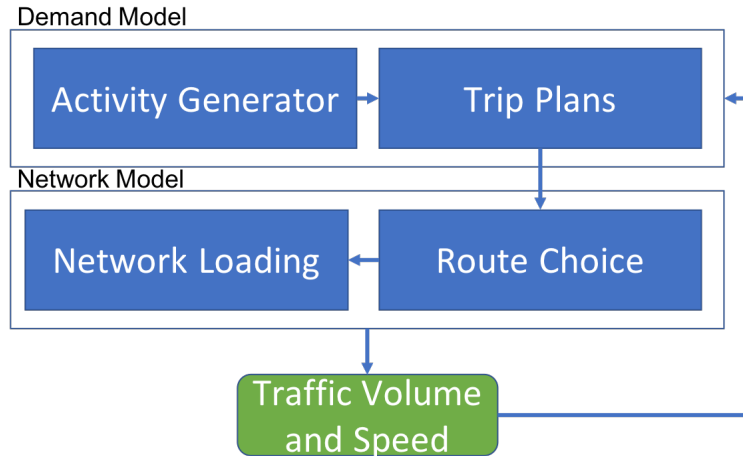


Figure 1: An example of simulation flow diagram for an integrated transportation simulator

Typically, the demand-network models are executed several times in a loop to achieve an approximation to equilibrium in the network flows. The traffic volume and speed are the main outputs of the simulator that are used in our calibration procedure by comparing with the measured traffic flows.

2.1 Demand Module

A demand module first generates a set of trips for each of the travelers (agents) by first assigning a destination and series of choices to individual users. For POLARIS, a Weibull hazard model is used [4] to estimate the probability $h_{ij}(t)$ of an activity of type j occurring for traveler i at time t :

$$h_{ij}(t) = \gamma_j t^{\gamma-1} \exp(-\beta_j^T x_i), \quad (2)$$

where γ_j is the shape parameter of the Weibull distribution, x_i are observed attributes of the traveler and β are the model parameters estimated from a survey.

Next, the order and timing for each activity, such as location, start time, duration and mode, is allocated by the trip planning model which is a set of discrete choice models; POLARIS uses the multinomial logit model [11] to choose the destinations for each given activity type. This model is derived from random utility maximization theory, which states that for each decision maker n and location i , there is a utility U_{in} associated with selecting location i . A generalized linear model for utility is assumed

$$U_{in} = \beta^T x_{ni} + \epsilon_{in}, \quad (3)$$

where β_i represent the parameters estimated from survey data; x_{ni} are observed attributes of traveler n and location i , such as travel time to, and land use attributes of, i ; and ϵ_{in} is an unobservable random error which follows a Gimbel distribution so that the probability of traveler n choosing destination i is given by

$$p_n(i) = \exp(V_{in}) / \sum_{j \in C_n} \exp(V_{jn}) \quad (4)$$

Here $V_{in} = \beta^T x_{ni}$. The choice set C_n is formed using a space-time prism constraint [3].

Once attributed, the planning order is determined using the Ordered Probit model, which is an extension of the basic probit model for binary responses extended to ordinal responses $y \in \{1, \dots, K\}$. Under this model, the probability of y being equal to k is given by

$$p(y = k) = p(l \leq \alpha_k) - p(l \leq \alpha_{k-1}),$$

where $\alpha_1, \dots, \alpha_{K-1}$ is a set of threshold-values, and $l = \beta^T x + \epsilon$, $\epsilon \sim N(0, \Sigma)$.

2.2 Network Module

Once the trips, defined by the origin, destination, departure time and mode, are generated, the network model performs Dijkstra's algorithm to determine route on the transportation network. Once these choices on routes are selected, destination and departure times are assigned to each agent and the resulting congestion levels within the road network is produced. Kinematic Wave theory of traffic flow [73] is used to simulate traffic flow on each road segment. This model has been recognized as an efficient and effective method for large-scale networks [59] and dynamic traffic assignment formulations.

In particular, the Lighthill-Whitham-Richards (LWR) model [57, 76] along with discretization scheme proposed by Newell [73] is used. The LWR model is a macroscopic traffic flow model. It is a combination of a conservation law defined via a partial differential equation and a fundamental diagram. The fundamental diagram is a flow-density relation $q(x, t) = q(\rho(x, t))$. The nonlinear first-order partial differential equation describes the aggregate behavior of drivers. The density $\rho(x, t)$ and flow $q(x, t)$, which are continuous scalar functions, satisfy the equation

$$\frac{\partial \rho(x, t)}{\partial t} + \frac{\partial q(x, t)}{\partial x} = 0.$$

This equation is solved numerically by discretizing time and space.

In addition, intersection operations are simulated for signal controls, as well as stop and yield signs. The input for LWR model is a fundamental diagram that relates flow and density of traffic flow on a road segment. The key parameter of fundamental diagram is critical flow, which is also called road capacity. The capacity is measured in number of vehicles per hour per lane, and provides theoretical maximum of flow that can be accommodated by a road segment.

3 Bayesian Model Formulation

An activity-based transportation simulator runs are computationally expensive and thus a limited number of simulation runs can be carried out. The problem of calibration is formulated as an optimisation problem with the objective of minimizing the difference between the observed flows y and simulated flows $\eta(\theta)$:

$$\theta^* \in \arg \min_{\theta \in A} \mathcal{L}(y, \eta(\theta)) \quad (5)$$

Here the constraint set A represents a modeler's prior knowledge about feasible ranges of the activity-based model parameters. Without loss of generality we omit the static variable z that is known to the models and does not need to be calibrated. The goal is to find an optimal value of θ which will align the simulator's predicted outputs with the true process.

The form of the loss function \mathcal{L} depends on the observation error term e , and a systematic error term accounting for the difference between the model output and the traffic observations $\epsilon(\theta)$. Assuming both of the error terms to be Normal with zero mean, we get the least-squares loss function

$$\mathcal{L}(y, \eta(\theta)) = \|y - \eta(\theta)\|_2^2$$

In our application we use traditional Bayesian optimisation approach for model calibration. We start with ensemble of initial simulator runs at N input setting $\theta_1, \dots, \theta_N$ and then, using the set of input-output pairs $\theta_i, \mathcal{L}(y, \eta(\theta_i))$, a Bayesian statistical model is formulated to capture the input-output relationship. Each additional sample recommended for evaluation is then iteratively chosen using the sequential design of experiment paradigm; the loss function is evaluated according to a chosen heuristic to determine the optimal next sample which has the greatest potential for improving the estimated solution [68].

We use a Gaussian Process (GP) to model the value of the loss function at new locations θ and to perform the sequential design of experiment. One key component of our formulation is use of dimensionality reduction pre-processing to accelerate the search for optimal location. In this section we describe the dimensionality reduction and Bayesian optimisation techniques we propose to solve the problem of calibrating a high-dimensional transportation simulator.

3.1 Exploratory Analysis of POLARIS Simulator Runs

We use $d = 5$ input parameters $\theta = [\theta_1, \dots, \theta_5]$ (Table 1) in order to demonstrate our framework. This parameters were identified by modeler as the most important to be calibrated.

Type	Name	Description	Range
Mode	HBO_B_male_taxi	Effect of traveler's sex on taxi utility	[0.298, 2.298]
Mode	NHB_B_dens_bike	Effect of population density on bike utility	[6.601, 8.601]
Mode	HBO_ASC_TAXI	Intercept in taxi utility	[2.34, 4.34]
Destination	THETAR_WORK	Effect of retail accessibility	[-8.553, -6.553]
Destination	GAMMA_SERVICE	Distance decay	[7.038, 9.038]

Table 1: Activity-Based model parameters and their lower and upper bounds

For each input parameter setting, 24 hours of simulated turn travel times, averaged over 5-minute intervals are taken as the simulator outputs. The resulting 288 outputs are used to calculate an objective function \mathcal{L} which is the mean squared error between simulated and observed values:

$$\mathcal{L}(\theta) = \frac{1}{288} \sum_{i=1}^{288} (y_i - \eta(\theta)_i)^2. \quad (6)$$

To explore the nature of the input-output relations we use the Morris screening technique [82], which is widely used for high-dimensional models, to explore the non-linearity among the input-output relations and any interactions among the input parameters θ . Morris procedure starts by generating an initial set of

origin samples $\theta^{(1)}, \dots, \theta^{(r)}$. Each variable in $\theta^{(i)}$ is uniformly sampled from its corresponding range. A set of r trajectories are then built, where each trajectory starts at point $\theta^{(i)}$ and is generated by perturbing each of the d variables one at a time by fixed value δ . For our analysis we use $r = 6$ trajectories constructed by $d = 5$ steps, thus resulting in a sample of $N = 36$ input-output pairs.

Given this initial sample set, we calculate the finite difference with respect to this variable, called elementary effect (EE), for each trajectory i and each variable j :

$$EE_{i,j} = \frac{\mathcal{L}(\theta_1, \theta_2, \dots, \theta_j + \delta, \dots, \theta_m) - \mathcal{L}(\theta_1, \theta_2, \dots, \theta_j, \dots, \theta_m)}{\delta} \quad (7)$$

Then Morris procedure analyses elementary effects using three statistics

$$\mu_j = \frac{1}{r} \sum_{i=1}^r EE_{i,j}, \quad \sigma = \sqrt{\frac{1}{r} \sum_{i=1}^r (EE_{i,j} - \mu_j)^2}, \quad \mu_j^* = \frac{1}{r} \sum_{i=1}^r |EE_{i,j}|.$$

Where μ_j measures the average, overall influence of the input j on the output σ measures the aggregate degree of higher-order interactions between the i th factor and all other $i \neq j$ input factors, known as the standard deviation of the EE. Finally, μ_j^* is an adjusted version of μ_j to handle cases when positive and negative effects may cancel one another in μ by using the absolute values of EEs [17].

An importance of a variable then can be used by comparing μ and μ^* [82]. Variables with a high value of μ suggest a high level of importance and that the effect is monotonic while high values of μ^* with low μ values indicate non-monotonic and/or non-linear behavior. Variables with an equivalent value of 0 for both μ and μ^* have no effect on the output and can be discarded. A comparison of μ^* and σ provides information on non-linear and/or interaction effects. High proportions of σ to μ^* indicates that the variable interacts with other variables and/or the objective function is non-linear with respect to this variable. Low proportions indicates no interactions and linearity.

Figure 2(a) plots the values of calculated statistics for each of the five variables. All of the five variables have a positive value of μ^* and thus all of them have a significant effect on the output. Variables GAMMA_SERVICE and THETAR_WORK have the highest importance and influence on the objective function. The value of μ and μ^* are similar for THETAR_WORK, suggesting positive monotonic behavior; HBO_ASC_TAXI suggests a negative monotonic behavior but the right graph implies an influential non-linear component as well.

Figure 2(b) shows most of the variables have high values of σ , indicating strong interaction effects and/or non-linear behavior. While HBO_ASC_TAXI is comparatively lower, its ratio to μ^* remains high at 86% of μ^* . This indicates a significant interaction or non-linear effect on the other variables but with a lower direct influence on the overall output.

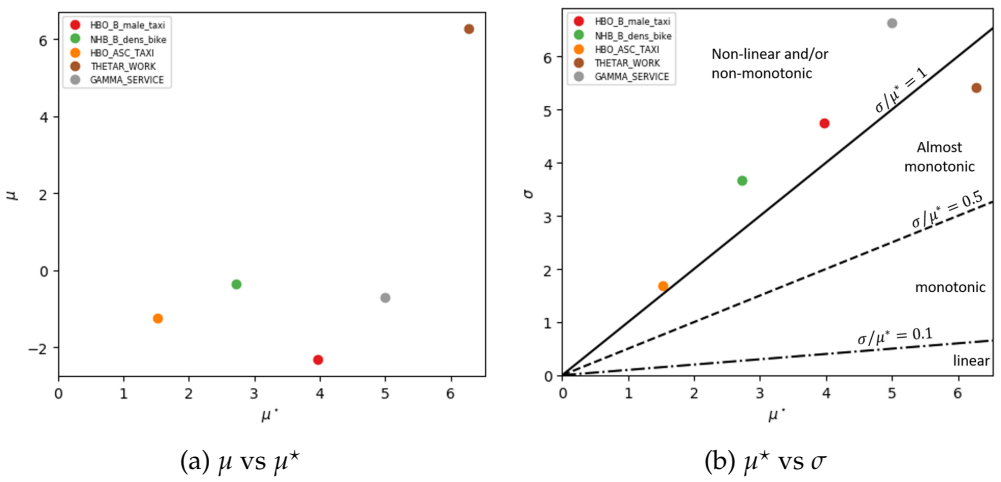


Figure 2: (a) A comparison of μ and μ^* [82] for importance ranking. Since no variable has a $\mu^* = 0$, all variables are significant. (b) A comparison of μ^* and σ . High values of μ^* with low μ values indicate non-monotonic and/or non-linear behavior while high values of σ indicate interactions.

In conclusion, all variables prove important and presence of interactions prevent us from using variable screening or shrinkage as dimensionality reduction technique. Further non-linear and non-monotonic nature of the input-output relations advise against using traditional projection-based dimensionality reduction methods.

3.2 Bayesian Optimization

The Bayesian optimisation procedure starts with an initial sample set \mathcal{D}_N . Simple random and Latin Hypercube (LHS) sampling are two common sample generating procedures used in computer simulations [46]. Simple random sampling draws a uniformly-distributed random value from each individual variable's domain to construct a sample set but, though easier to implement, cannot guarantee that every portion of the subspace is sampled [46]. LHS first subsections each variable range into equal intervals and selects a random value within each slice before randomly pairing each variable's new subset to construct a sample [64]. Our Bayesian optimization procedure uses a LHS configuration to generate our initial sample set $\mathcal{D}_N = [\theta_1, y_1], \dots, [\theta_N, y_N]$.

A surrogate model is then estimated using a univariate Gaussian Process to quantify the uncertainty at other unsampled points in the domain; a GP is fully characterized by its mean function m and its covariance function, or kernel, k [43].

$$\mathcal{L}(e) \sim \mathcal{GP}(m(\theta), k(\theta, \theta')) \quad (8)$$

where

$$\begin{aligned} m(\theta) &= \mathbb{E}[\mathcal{D}_N | \theta] \\ k(\theta, \theta') &= \mathbb{E}[(\theta - m(\theta))(\theta' - m(\theta'))] \end{aligned} \quad (9)$$

The mean function $m(\theta)$ is unrestricted but, in practice, is routinely assumed to be zero. The correlation equation $k(\theta, \theta')$ must result in a positive semi-definite matrix; common choices include the Squared Exponential, which is both stationary and isotropic, and the Matérn covariance function, which provides less smoothness through the reduction of the covariance differentiability. General references can be found in [1] and [33]. In this paper, we use the Matérn covariance function:

$$k_{\text{Matern}}(x, x') = \frac{2^{1-v}}{\Gamma(v)} \left[\frac{\sqrt{2v}|x - x'|}{\lambda} \right]^v K_v \left[\frac{\sqrt{2v}|x - x'|}{\lambda} \right]$$

where Γ is the gamma function, K_v is a modified Bessel function, and λ and v are non-negative hyperparameters for lengthscale and smoothness respectively.

Additionally, we incorporate the observational and residual errors of $e \sim \mathcal{N}(0, \sigma^2)$ in Equation 1 via a specialized Linear 'nugget' kernel [42]:

$$\mathcal{L}(e) \sim \mathcal{GP}(m(\theta), K = k(\theta, \theta') + r(\theta)) \quad (10)$$

where $r(\theta) = \sigma_e^2 \delta_{\theta, \theta'}$ and $\delta_{x, x'}$ is the Kronecker delta.

Once conditioned on the observed data \mathcal{D}_N , the final density known as the posterior distribution, is Normal:

$$[y(\theta) \mid \mathcal{D}_N = [\Theta_N, Y_N], \theta, \Omega] \sim \mathcal{N}(\mu(\theta), \Sigma(\theta)) \quad (11)$$

with the following summary statistics:

$$\begin{aligned} \mu(\theta) &= m(\theta) + k(\theta)(K_{\mathcal{D}})^{-1}[Y_N - m(\Theta_N)] \\ \Sigma(\theta) &= k(\theta, \theta) + r(\theta) - k(\theta)(K_{\mathcal{D}})^{-1}k(\theta)^T \end{aligned} \quad (12)$$

where $k(\theta) = (k(\theta, \theta_1), \dots, k(\theta, \theta_N))^T$ and Ω are the parameters of the kernel function.

The next step of the procedure is sequential sampling of the input configurations and updating the parameters of the GP surrogate. Under limited sampling budgets, choosing the next configuration for evaluation θ^{N+1} using the *optimal experimental design*. The goal is to identify regions of the state space \mathcal{A} to draw from where the loss function \mathcal{L} is known to have small values (exploitation) or in the regions of high uncertainty about values of the loss function (exploration). The next configuration is chosen using a utility function U depending on the exploration-exploitation trade-off required for the given application. The expectation over the utility function, known as acquisition function, is taken over the posterior distribution of the GP surrogate function and minimized to obtain the optimal design choice [79]:

$$\theta^{N+1} = \arg \max_{\theta \in \mathcal{A}} \mathbb{E}[U(\theta, \Omega)] \quad (13)$$

where θ^{N+1} is the optimal design configuration, decision from the potential candidates in the search space \mathcal{A} ; U is the chosen utility function, and Ω represents the hyperparameters of the surrogate that approximates the loss function \mathcal{L} .

[19] discusses extensively several Bayesian utility functions and their non-Bayesian Design of Experiments (DOE) equivalents but this paper focuses on Expected Improvement [68], which emphasizes the size of the improvement to avoid getting stuck in local optimas and under-exploration.

$$EI(\theta^*) = K_{post}(\theta^*)[u\Phi(u) + \phi(u)] \quad (14)$$

where $u = \frac{L(\theta^+) - \mu_{post}(\theta^*)}{K_{post}(\theta^*)}$; $\Phi(\cdot)$ is the normal cumulative distribution; $\phi(\cdot)$ is the normal density function, and $\mathcal{N}(L; \mu_{post}, K_{post})$ is the predictive posterior distribution.

3.3 Dimension Reduction

Although GP surrogates approximate well non-linear relations between inputs and simulator outputs, they are known to fail in higher dimensions. Dimensionality influences the state-space volume exponentially and in order for Bayesian Optimisation (BO) to maintain reasonable uncertainty in predictions, this "curse of dimensionality" mandates an exponential growth in sample sizes. Parallelization, while able to augment a limited sampling budget, can only provide a multiplicative expansion; furthermore, when high enough samples are produced, additional computational complexity within the algorithm itself becomes a hindrance. For this reason, BO is an ineffective beyond a moderate level of high-dimensional complexity [80]. However, if the dimensionality issue can be addressed, BO might become applicable.

On the other hand, in many engineering applications, the relations between inputs and outputs vary primarily along a few non-linear curves. Then those curves are linear, one may use projection based techniques, such as principal component analysis, partial least squares or single-index models. Projection-based dimensionality reduction techniques have traditionally been implemented due to their computational and

interpretable ease. One such technique, popular in engineering disciplines, known as Active Subspaces (AS) projects the data along influential directions known as Principal Components (PCs). Utilizing derivatives, the algorithm identifies the necessary linear combinations to produce a lower-dimensional subspace. For further details of Active Subspaces, see Appendix A.

As we demonstrated in Section 3.1, relations in our applications are non-linear and include interactions, and thus, require non-linear dimensionality reduction techniques. We propose a nonlinear extension of the projection-based methods by projecting the input θ onto a non-linear surface instead of a linear space. Our dimensionality reduction procedures finds a map $\phi(\theta) \rightarrow \psi$ that transforms the input vector θ into a lower-dimensional vector of latent variables ψ . We propose, using *neural networks* to construct a nonlinear mapping ϕ . Our paper will use Active Subspaces as a benchmark for demonstration.

Each step of an optimisation algorithm requires evaluation of the loss function and thus, requires running a simulator. Therefore, our dimensionality reduction technique has to be able to reconstruct a point in the original input space from the point in the latent space. Further, the re-sampling step of the BO requires the latent space to be bounded.

Performing reconstruction requires the inversion of a non-linear map, which makes this task non-trivial, and has resulted in linear approximation techniques dominating the field of dimensionality reduction, despite commonly mapping non-linear relationships [55]. This paper, however, asserts that this translation obstacle is surmountable for deep learning methodologies and can provide an advantageous alternative to popular linear methods within the established optimization framework.

In order to provide a bidirectional translation, we combine a feed-forward multi layer perceptron (MLP) architecture, which will capture a low-dimensional representation of the input-output, with an Autoencoder architecture, which will capture a low-dimensional representation of the input-input. The Autoencoder and MLP share the same initial layers up to the reduced dimension layer, as shown in Figure 3, in order to enforce they both use the same encoding substructure. The final architecture is

$$\hat{\mathcal{L}}(\theta) = F(\phi(\theta)) \text{ (MLP)} ; \quad \hat{\theta} = s(\phi(\theta)) \text{ (Autoencoder)}$$

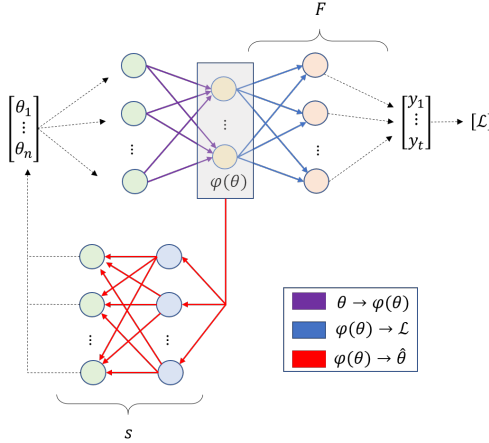


Figure 3: Graphical Representation of the Combinatorial Neural Network for Calibration

The joint training of the encoder and decoder allows us to efficiently perform cross validation on the dimensionality of the latent space. This is accomplished through a combined loss function that takes into account both the errors in the predicted output loss values $\hat{\mathcal{L}}$ and the reconstructed input values $\hat{\theta}$. Though any loss function which captures these errors can be used, this paper uses the following loss function $l_{NN} = M_\lambda + Ap$:

The MLP portion, mapping the input θ to the output's loss function \mathcal{L} , of the architecture uses the Mean

Squared Error (MSE) function multiplied by a scalar λ ¹:

$$M_\lambda = \lambda \sum_{i=1}^N (\mathcal{L}_i - \hat{\mathcal{L}}_i)^2 \quad (15)$$

The Autoencoder portion A_P of the loss uses the mean squared error function and a summed quadratic penalty cost P for producing predicted values outside of the original subspace bounds:

$$A_P = \sum_{i=1}^N \left[(\theta_i - \hat{\theta}_i)^2 + P \left(\max[0, \hat{\theta}_i - \theta_{ui}]^2 + \max[0, \theta_{li} - \hat{\theta}_i]^2 \right) \right] \quad (16)$$

where θ_u represents the input set's upper bound, and θ_l represents the input set's lower bound.

Due to the bounded requirement of BO, some activation functions will require adjustments for at least the dimension reducing bottleneck layer. For example, the ReLU function can be bounded by adjusting the neural network to add two new parameters defining the state space bounds DR_{ub}, DR_{lb} :

$$U(\theta^{N+1}) = \begin{cases} DR_{lb}, \theta < DR_{lb} \\ \theta, DR_{lb} \leq \theta \leq DR_{lb} \\ DR_{lb}, \theta > DR_{lb} \end{cases} \quad (17)$$

When constructing the neural network architecture, the user should consider that any artificial bounding can result in the need for additional nodes and/or layers when compared with an unbounded version.

Each of the functions in this dimensionality reduction architecture ϕ , F , and s is a neural network. Neural Networks (NN) are a class of non-linear functions which construct a predictive mapping using hierarchical layers of latent variables. The output can be a continuous, discrete, or mixed value set. Each layer ℓ applies element-wise a univariate activation function τ to an affine transformation:

$$\begin{aligned} Z^{(1)} &= \tau^{(1)} \left(W^{(0)} \Theta + b^{(0)} \right), \\ Z^{(2)} &= \tau^{(2)} \left(W^{(1)} Z^{(1)} + b^{(1)} \right), \\ &\dots \\ Z^{(\ell)} &= \tau^{(\ell)} \left(W^{(\ell-1)} Z^{(\ell-1)} + b^{(\ell-1)} \right), \\ \hat{Y} &= W^\ell Z^\ell + b^{(\ell)} \end{aligned} \quad (18)$$

where W represents the weights placed on the layer's input set Z , and b represents the offset value critical to recovering shifted multivariate functions.

Networks consisting of multiple layers are referred to as a Deep Neural Network (DNN); given the number of layers ℓ , a predictor then becomes the composite map

$$\hat{\mathcal{L}} := \left(\tau_1^{W_1, b_1} \circ \dots \circ \tau_\ell^{W_\ell, b_\ell} \right) (\theta) \quad (19)$$

Neural network given by Equation (19) is known as Multi-Layered Perceptron (MLP). A specialized variation, known as a Autoencoder maps the input to itself via a bottleneck structure, which means the model aims to concentrate information required to recreate θ using a latent vector Z .

The general approximation capabilities of neural networks is rooted in the universal basis theorem proved by Kolmogorov [54].

As data progresses down the network, each layer applies a folding operator to predecessor's divided space according to the chosen activation function τ . Cybenko[27] proved that a fully-connected network with a single hidden layer and sigmoid activation function can uniformly approximate any continuous multivariate function on a bounded domain within an error margin; further work documented similar results for additional classes of activation functions [9, 49, 38] and eventually led to neural networks being deemed universal approximators: a single-layered neural network with a suitable activation function for continuous functions; a two-layered version for discontinuous and Boolean functions.

¹This is to adjust importance for or against the encoder verses the decoder

3.4 Parallelization

Traditional Bayesian optimization algorithms are sequential in nature [50]; however, several recent approaches address the problem of parallel evaluations [100, 25, 29, 87, 98] using High Performance Computing (HPC). When simulation runs take hours or days, "batching" of samples become critical to optimization efforts.

We developed a computational framework that consists of an HPC master controller program which coordinates worker units to run codes across multiple processors concurrently; the result being a larger set of unknown inputs to be evaluated in an acceptable time frame. For this optimization framework, the controller must also interact with a model exploration program for its queue of untested input sets, as shown in Figure 4.

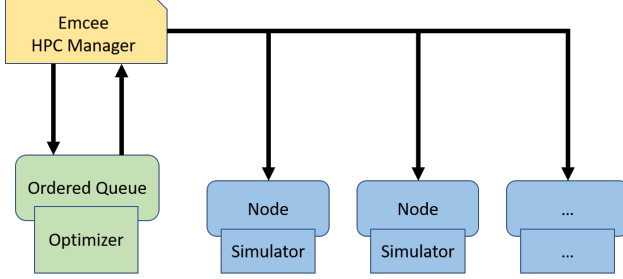


Figure 4: Computation Framework for HPC

In direct consequence of parallelism, BO must also be adjusted to recommend multiple samples. A natural approach may seem to be simply choosing the top c candidates of the acquisition function. However, the problem with such an approach lies in the assumption that the top set of points depict unique sections of the search space and are not clustered together. It is not uncommon that, when a new portion of the search space is deemed worth exploring, many of the candidates in that region will contain a large acquisition value, as they all are deemed equally valuable for learning the area's structure.

Instead, the expected information gained from evaluating a selected candidate in the batch can be leveraged when deciding the next option. In this approach, the posterior distribution is updated with a pseudo-sample created from the predicted mean for the chosen candidate. The expected "information gain" prevents additional candidates from clustering; the predicted posterior mean for a candidate is taken as the "simulated" value and the posterior distribution for all other candidates are updated before another candidate is chosen.

While proven successful enough to be the most common method implemented[100], this expectation method is not the only possible recourse. Recently, more complex methods have begun to be explored that may prove, in some optimization scenarios where batch sizes are expected to be very large, to be more useful:

- Gradient applications which choose the next sample by maximizing the expected incremental value[100], value of information[101], or other methods of diversity measurements[5]
- Utilizing the lower bound for the previously-chosen but yet-to-evaluate samples[101]
- Partitioning the search space via some design such as treed maximum entropy and selecting candidates from each region proportional to the volume in the region [41]
- Performing Monte-Carlo simulation to estimate the posterior distribution over examples selected by the sequential method and then select a batch of c examples that "best matches" this distribution; however, no theoretical results prove convergence[5]

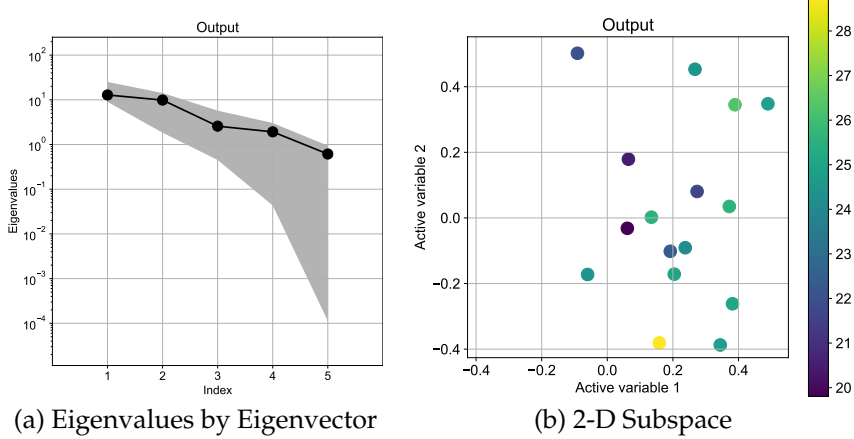


Figure 5: (a) Eigenvalues for each variable Eigenvector (black circles) and accompanying Bootstrap Interval (grey regions) found using 1000 bootstrap replicates. (b) Training samples projected onto the 2-D active subspace.

4 Empirical Results

We apply our methodology to minimize the objective loss function \mathcal{L} , which is the mean squared difference between the observed and simulated turn travel times for every 5-minute interval across a 24-hour period.

All variables not being calibrated are assumed to be known. We generate an initial sample of size 16 which is used to estimate the parameters of our dimensionality reduction maps as well as the parameters of the mean function. The initial sample was generated via Latin Hypercube. Then we apply BO algorithm using the Expected Improvement (EI) utility criterion with batch-size of 2. We compare the performance of multiple configurations of our framework. Specifically we evaluated the following dimensionality reduction configurations:

- **Original (Orig)**- no dimensionality reduction
- **Active Subspace (AS)** - the 2-dimensional subspace resulting from the Active Subspace dimensionality reduction pre-processing outlined in Appendix A
- **Neural Network (NN)** - the 3-dimensional subspace resulting from the neural network dimensionality reduction pre-processing

Then we combine each of the dimensionality reduction configuration with one of the two GP profiles: a zero-mean GP \mathcal{GP}_0 , and a neural network-adjusted mean GP \mathcal{GP}_{NN} . Both instances use a Matérn covariance function.

4.1 Configurations

The choice of latent space dimensionality for the AS algorithm was determined from the elbow plot shown in Figure 5(a) which shows the eigenvalues and the 95% confidence interval calculated from 1000 bootstrap samples.

The gap between the second and third variables indicate the likely presence of a 2 dimensional active subspace, which is supported by Figure 5(b). Notably, the bounds in the bootstrap intervals are quite large; however, given that the bootstrap intervals are most bias at low sample numbers, this outcome is not unexpected.

A 3-dimensional subspace was constructed for the NN dimension reduction using the structure visualized in Figure 6.

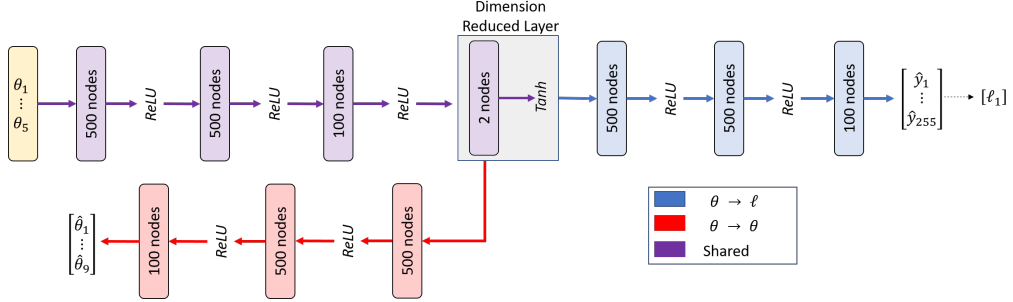


Figure 6: The implemented NN structure for calibration. Rectangles represent the number of affine transformations applied to their layer inputs.

A *ReLU* function was applied universally with the exception of the reduced dimension layer, which utilized a *tanh* transformation to enforce a range boundary. The network was trained on 1000 epochs with a loss function \downarrow_{NN} using a penalty value $P = 200$ for decoding outside the original subspace bounds and a scalar $\lambda = 0.005$ in order to encourage equal consideration between learning the decoding and encoding structures:

$$l_{NN} = 0.005\|Y - \hat{Y}\|_F + \|\theta - \hat{\theta}\|_F + 200 \sum_{i=1}^N \left[\max[0, \hat{\theta}_i - \theta_{ui}]^2 + \max[0, \theta_{li} - \hat{\theta}_i]^2 \right] \quad (20)$$

Each subspace used the same NN mean structure for the modified BO GP, depicted in 7.

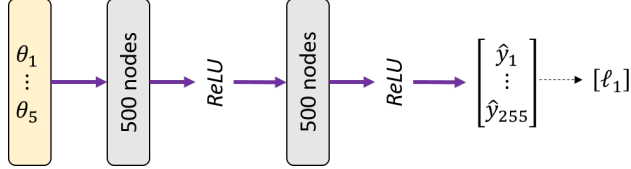


Figure 7: The implemented network structure of the adjusted mean function. The rectangles represent the affine transformations applied to their layer inputs.

A *ReLU* function was applied universally and the network was trained on 800 epochs with a learning rate of 0.01; a simple MSE loss function was used.

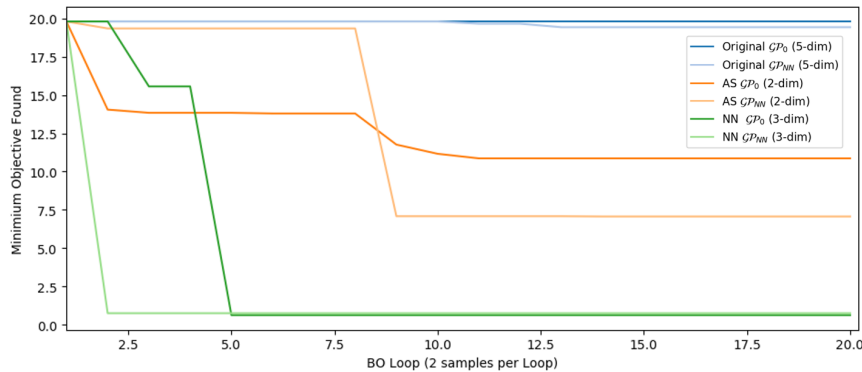


Figure 8: Comparison of the minimum objective value found in 20 BO iterations by each configuration during the calibration of 5 dimensions.

Although vanilla BO is applicable to 5-dimensional problems, the highly non-linear and heteroskedastic nature of our problem makes BO impractical. The vanilla BO yields no improvements after 20 iterations. When the non-zero NN mean was used, the BO only manages an 2% improvement after 12 iterations.

The AS + \mathcal{GP}_0 configuration achieves a 30% objective reduction within the first iterations; within 10 iterations, it ultimately settles at an objective value of 10.86 for a total improvement of 45% and then stagnates. Adding a \mathcal{GP}_{NN} mean improves on the $AS\mathcal{GP}_0$ result by 35%, leading to a final objective value of 7.07 and a 65% final improvement on the initial solution. However, it required 6 more iterations for AS + \mathcal{GP}_{NN} to achieve the improvement.

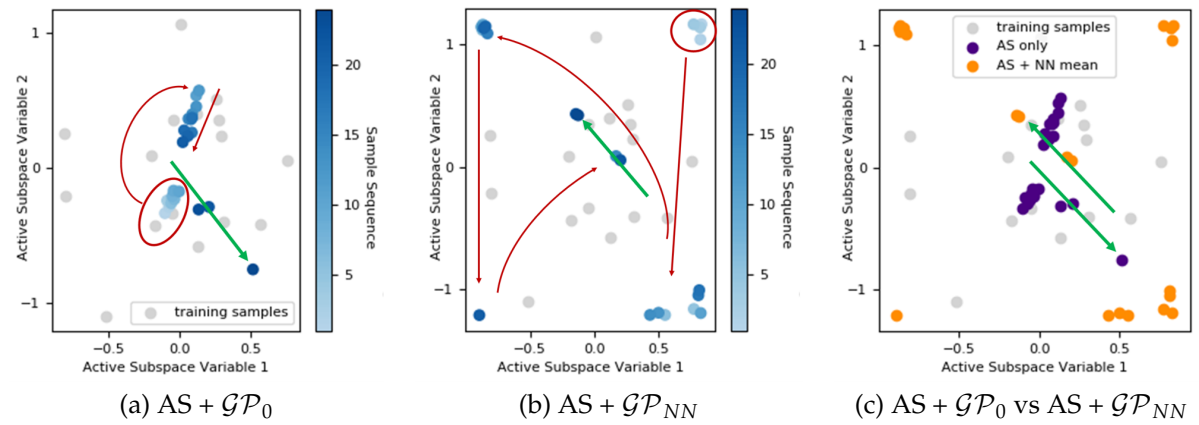


Figure 9: Samples in latent subspace that were used by the search algorithm. The grey dots correspond to the initial 16 samples and the 40 colored dots were sequentially recommended in over the 20 BO iterations. The intensity of the blue color corresponds to the order in which the samples were recommended. The red circles are initial recommendations, the red arrows show the sampling directions, and the green arrow highlights the final trajectory. (a) AS + \mathcal{GP}_0 (b) AS + \mathcal{GP}_{NN} (c) overlays (a) in purple and (b) in orange to highlight that the final trajectories are parallel but offset.

4.2 Results

Figure 9 shows that the use of the \mathcal{GP}_{NN} leads to more exploration by the search algorithm. While, AS + \mathcal{GP}_0 primarily employed exploitation of the initial training set, recommending samplings within a tight cluster about the majority of the training points in the center of the subspace, the AS + \mathcal{GP}_{NN} explored the unknown portions of the search space.

Typically, the change in behavior would imply that the Expected Improvement (EI) acquisition function faced higher variance due to the NN mean as, broadly, EI encourages exploitation when a strong reduction in the mean function is predicted and exploration when the variance is high. However, as shown in Figure 10, this is not the case.

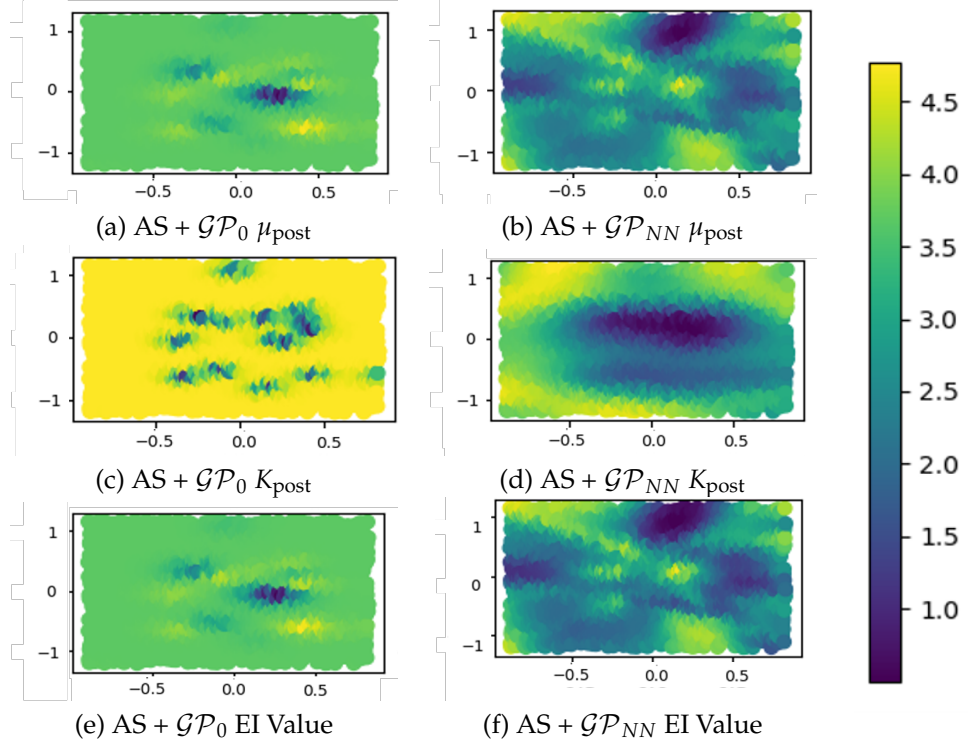


Figure 10: Expected Improvement components and acquisition values for candidate points in the AS statespace during an interval of the BO calibration for AS + \mathcal{GP}_0 (a)(c)(e) and AS + \mathcal{GP}_{NN} (b)(d)(f). (a) and (b) show the predicted mean reduction component, (c) and (d) show the predicted standard deviation component, and (e) and (f) show the final acquisition calculation result. The acquisition function in both settings rely heavily on the mean reduction component despite their diverging recommendation patterns.

Both \mathcal{GP}_0 and \mathcal{GP}_{NN} acquisition values clearly rely heavily on the potential in mean reduction. Instead, it is the landscape of the predicted mean and uncertainty which shifts significantly. This outcome is likely due to the newly reflected magnitude of non-linear behaviors previously unaddressed by the AS + \mathcal{GP}_0 configuration. Figure 9(c) shows this to indeed be the case, where the AS + NN_GP required an offset to locate improved recommendations.

The largest advancement was produced by the NN + \mathcal{GP}_0 configuration at 96% with a final objective value of 0.75; furthermore, this achievement was located within just 3 iterations. The addition of the \mathcal{GP}_{NN} netted a similar reduction but accelerated the search to within the first iteration. Table 2 provides summary findings.

Reduction Technique	Minimum Objective Value Found	Found by BO at Iteration Number	Improvement over Initial Solution
Initial	19.802	-	-
Original (5-D) + 0 - GP	19.802	20	0.00%
Active Subspaces (2-D) + 0 - GP	10.86	10	45.15%
Neural Network (3-D) + 0 - GP	0.625	4	96.85%
Original (5-D) + NN - GP	19.427	12	1.89%
Active Subspaces (2-D) + NN - GP	7.07	13	64.32%
Neural Network (3-D) + NN - GP	0.75	1	96.21%

Table 2: Comparison by configuration of their best solutions found during a maximum of 20 BO iterations. Each iteration produced 2 recommendations for evaluation.

4.3 Predictions

In this section, we review the improvements made to the simulation outputs as a result of the calibration process. We treat the best of the initial 16 LHS samples as a baseline to compare with the NN + \mathcal{GP}_0 solution.

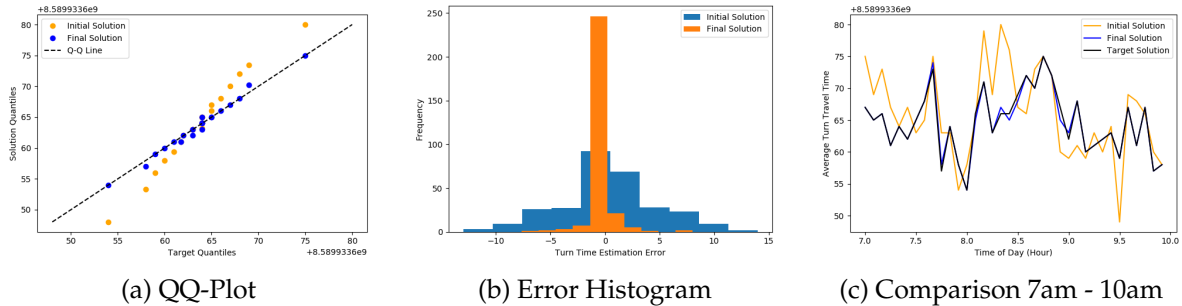


Figure 11: Comparison of the targeted outputs with the initial solution found during the 16 initial sample set and the final solution found by NN + \mathcal{GP}_0 during the 20 iterations of BO. (a) compares each solution’s Quantiles to the targeted solution’s Quantiles. The black, dashed line indicates where the ideal solution should lie. (b) captures the distribution of output errors between the solutions and the targeted solution. (c) shows the average turn times around and at rush hour (7 am - 10 pm)

Figure 11(a) takes a non-parametric approach to compare the solutions in respect to the targeted outputs via a Quantile-Quantile (Q-Q) plot. The plot shows the initial solution aligning in the central quantiles but curving off on either side while the calibrated solution remains in consistent alignment. This indicates that the initial solution was heavy-tailed, or possessed more extreme values than the true solution, and that the calibration process was able to correct the behavior. Figure 11(b) further highlights this accomplishment. The calibrated solution is shown to not only improve the frequency of correct outputs but tighten the initial solution’s extreme deviations.

5 Discussion

We provided a Bayesian optimization framework for complex transportation simulators. We have shown that Bayesian optimization algorithms when combined with dimensionality reduction techniques is good

default option for calibration of activity based simulators. Bayesian approach provide several advantages over other black-box optimization techniques:

1. Distribution over functions provide a clear approach to the active learning problem (sequential design of computational experiment).
2. The posterior distribution allows for sensitivity analysis and uncertainty quantification to be performed.

Although Bayesian optimization has been proposed before for simulation-based problems, our approach that combines it with dimensionality reduction techniques allow to solve real-life high-dimensional problems. Our parallel batching strategy and high performance computing framework allow for this approaches to be used by both researchers and transportation practitioners.

A Active Subspaces

Active Subspaces (AS) identifies a linear transformation of the subspace by constructing a set of uncorrelated eigenvectors, known as Principal Components (PCs), defining the "active" subspace. These orthogonal directions, denoted as W , capture the average variability of the θ -to- \mathcal{L} relationship via a differential function $\mathcal{L} \approx f(\theta) : \mathbb{R}^d \rightarrow \mathbb{R}$:

$$\max_{\|W\|=1} \mathbb{E} [\|\mathcal{L}(\theta W)\|_0] \quad (21)$$

$$\mathbb{E} [W^T \theta^T \mathcal{L}^T \mathcal{L} \theta W] \quad (22)$$

$$W^T \mathbb{E} [\text{cov}^2(\theta V, \mathcal{L})] W \quad (23)$$

$$W^T C W \quad (24)$$

Given a bounded probability density function $\rho(\theta) \in \mathbb{R}^d$ on $f(\theta)$, AS first decomposes the eigenvalue-eigenvector representation on the gradient ∇_θ :

$$C = \int (\nabla_\theta f)(\nabla_\theta f)^T \rho(\theta) d\theta = \mathcal{W} \Lambda \mathcal{W}^T \quad (25)$$

where C is a sum of semi-positive definite rank-one matrices, \mathcal{W} is the matrix of eigenvectors, and Λ is the diagonal matrix of eigenvalues in decreasing order.

In cases where the gradient is unknown, as with most simulations, C can instead be approximated using an observed set of n inputs sampled from $\rho(\theta)$ via Monte Carlo:

$$\hat{C} = \frac{1}{n} \sum_{i=1}^n (\hat{\nabla}_\theta f_i)(\hat{\nabla}_\theta f_i)^T = \hat{\mathcal{W}} \hat{\Lambda} \hat{\mathcal{W}}^T \quad (26)$$

where $\hat{\nabla}_\theta$ is the observed gradient or an estimated gradient, such as a local or global linear regression models:

$$\begin{aligned} f_i &\approx \hat{\beta}_0 + \hat{\beta}^T \theta_i \\ \nabla_\theta f_i &= \hat{\beta} \end{aligned} \quad (27)$$

Once determined, the PCs are plotted on a log-scale and a dramatic drop in the eigenvalue space, documented as a *gap*, is sought²:

²if no gap can be found, compiling larger sets of eigenvalues or sampling more within the current eigenvalue framework to increase the eigenvalue accuracy is suggested

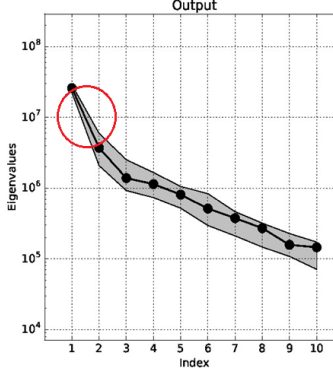


Figure 12: The largest eigenvalue gap is designated by a red circle

The dimensions $q < d$ to the left of the largest eigenvalue gap is designated the "active" subspace $v = \hat{\mathcal{W}}_1^T \theta$; the remaining $d - n$ directions define the "inactive" subspace $z = \hat{\mathcal{W}}_2^T \theta$.

$$\theta = \hat{\mathcal{W}} \hat{\mathcal{W}}^T \theta = \hat{\mathcal{W}}_1 v + \hat{\mathcal{W}}_2 z \quad (28)$$

The variables of z are then fixed at nominal values and the active set $\hat{\mathcal{W}}_1$ subsequently becomes the approximate representation of Θ :

$$\begin{aligned} f(\theta) &\approx \int f(\hat{\mathcal{W}}_1 v + \hat{\mathcal{W}}_2 z) p(v | z) dv \\ &\approx g(v) = g(\hat{\mathcal{W}}_1^T \theta) \end{aligned} \quad (29)$$

For more information behind the derivation of this procedure and its variations, see [24].

Like PCA, AS will require a subsequent, separate regression from the subspace to the output variables $v \rightarrow f(\theta)$:

$$f(\theta) = \beta \theta + \epsilon \quad (30)$$

$$\approx \beta v + \epsilon \equiv \beta \mathcal{W}_1^T \theta + \epsilon \quad (31)$$

Active Subspaces will provide results closer in line with Partial Least Squares (PLS). This is because, through leveraging the derivatives, the method actively prioritizes those directions which are also relevant to the input-output relationship ultimately being sought. However, the inversion of the lower-dimensional subspace to recover the original variables is complicated by the inactive subspace. For situations in which the inactive eigenvalues are exactly zero, $f(\theta)$ can be reconstructed without regard to the inactive subspace by setting $z = 0$:

$$f(\theta) \approx f(\hat{\mathcal{W}}_1 v) = f(\hat{\mathcal{W}}_1 \hat{\mathcal{W}}_1^T \theta) \quad (32)$$

When the inactive eigenvalues are small but not zero, decoding should be constructed by optimizing over the inactive subspace v such that:

$$\underset{v \in V}{\text{minimize}} \left[\underset{z \in Z}{\text{minimum}} \quad f(\hat{\mathcal{W}}_1 v + \hat{\mathcal{W}}_2 z) \right. \\ \left. \text{s.t.} \quad \Theta_{lb} - \hat{\mathcal{W}}_1 v \leq \hat{\mathcal{W}}_2 z \leq \Theta_{ub} - \hat{\mathcal{W}}_1 v \right] \quad (33)$$

where Θ_{lb} and Θ_{ub} are the lower and upper bounds of the original Θ state-space, respectively.

References

- [1] Petter Abrahamsen. *A Review of Gaussian Random Fields and Correlation Functions*. April 1997.
- [2] Kofi P. Adragni and R. Dennis Cook. Sufficient dimension reduction and prediction in regression. *Philosophical Transactions of the Royal Society A: Mathematical, Physical and Engineering Sciences*, 367(1906):4385–4405, November 2009.
- [3] Joshua Auld, Michael Hope, Hubert Ley, Vadim Sokolov, Bo Xu, and Kuilin Zhang. POLARIS: Agent-based modeling framework development and implementation for integrated travel demand and network and operations simulations. *Transportation Research Part C: Emerging Technologies*, 64:101–116, 2016.
- [4] Joshua Auld, Taha Hossein Rashidi, Mahmoud Javanmardi, and Abolfazl (Kouros) Mohammadian. Dynamic Activity Generation Model Using Competing Hazard Formulation. *Transportation Research Record*, January 2011. Publisher: SAGE PublicationsSage CA: Los Angeles, CA.
- [5] Javad Azimi, Alan Fern, Xiaoli Z Fern, Glencora Borradaile, and Brent Heeringa. Batch Active Learning via Coordinated Matching. page 8, 2012.
- [6] Dmitry Babichev and Francis Bach. Slice inverse regression with score functions. *Electronic Journal of Statistics*, 12(1):1507–1543, 2018.
- [7] Ramachandran Balakrishna, Moshe Ben-Akiva, and Haris N. Koutsopoulos. Offline Calibration of Dynamic Traffic Assignment: Simultaneous Demand-and-Supply Estimation, July 2003.
- [8] Simone Baldi, Iakovos Michailidis, Vasiliki Ntampasi, Elias Kosmatopoulos, Ioannis Papamichail, and Markos Papageorgiou. A Simulation-Based Traffic Signal Control for Congested Urban Traffic Networks. *Transportation Science*, 53(1):6–20, February 2019.
- [9] Andrew R. Barron. Approximation and estimation bounds for artificial neural networks. *Machine Learning*, 14(1):115–133, January 1994.
- [10] R. A. Bates, R. J. Buck, E. Riccomagno, and H. P. Wynn. Experimental Design and Observation for Large Systems. *Journal of the Royal Statistical Society: Series B (Methodological)*, 58(1):77–94, January 1996.
- [11] Moshe E. Ben-Akiva, Steven R. Lerman, and Steven R. Lerman. *Discrete Choice Analysis: Theory and Application to Travel Demand*. MIT Press, 1985. Google-Books-ID: oLC6ZYPs9UoC.
- [12] M. Binois, D. Ginsbourger, and O. Roustant. Quantifying uncertainty on Pareto fronts with Gaussian process conditional simulations. *European Journal of Operational Research*, 243(2):386–394, June 2015.
- [13] Mickael Binois, Robert B. Gramacy, and Michael Ludkovski. Practical heteroskedastic Gaussian process modeling for large simulation experiments. *Journal of Computational and Graphical Statistics*, 27(4):808–821, October 2018. arXiv: 1611.05902.
- [14] Andrew J Booker, JE Dennis, Paul D Frank, Virginia Torczon, and others. A Rigorous Framework for Optimization of Expensive Functions by Surrogates. 1998.
- [15] Eric Brochu, Vlad M. Cora, and Nando De Freitas. A tutorial on Bayesian optimization of expensive cost functions, with application to active user modeling and hierarchical reinforcement learning. *arXiv preprint arXiv:1012.2599*, 2010.
- [16] Tyson Browning. Applying The Design Structure Matrix To System Decomposition And Integration Problems: A Review And New Directions. *Engineering Management, IEEE Transactions on*, 48:292–306, September 2001.
- [17] Francesca Campolongo, Jessica Cariboni, and Andrea Saltelli. An effective screening design for sensitivity analysis of large models. *Environmental modelling & software*, 22(10):1509–1518, 2007.

[18] Ennio Cascetta and Sang Nguyen. A unified framework for estimating or updating origin/destination matrices from traffic counts. *Transportation Research Part B: Methodological*, 22(6):437 – 455, 1988.

[19] Kathryn Chaloner and Isabella Verdinelli. Bayesian experimental design: A review. *Statistical Science*, pages 273–304, 1995.

[20] Xi Chen, Matteo Diez, Manivannan Kandasamy, Zhiguo Zhang, Emilio F. Campana, and Frederick Stern. High-fidelity global optimization of shape design by dimensionality reduction, metamodels and deterministic particle swarm. *Engineering Optimization*, 47(4):473–494, April 2015.

[21] R.L. Cheu, X. Jin, K.C. Ng, Y.L. Ng, and D. Srinivasan. Calibration of FRESIM for Singapore expressway using genetic algorithm. *Journal of Transportation Engineering*, 124(6):526–535, November 1998.

[22] Linsen Chong and Carolina Osorio. A Simulation-Based Optimization Algorithm for Dynamic Large-Scale Urban Transportation Problems. *Transportation Science*, 52(3):637–656, July 2017. Publisher: INFORMS.

[23] Ernesto Cipriani, Michael Florian, Michael Mahut, and Marialisa Nigro. A gradient approximation approach for adjusting temporal origin–destination matrices. *Transportation Research Part C: Emerging Technologies*, 19(2):270–282, April 2011.

[24] Paul G. Constantine. *Active Subspaces: Emerging Ideas for Dimension Reduction in Parameter Studies*. Society for Industrial and Applied Mathematics, 2015.

[25] Emile Contal, David Buffoni, Alexandre Robicquet, and Nicolas Vayatis. Parallel Gaussian Process Optimization with Upper Confidence Bound and Pure Exploration. In David Hutchison, Takeo Kanade, Josef Kittler, Jon M. Kleinberg, Friedemann Mattern, John C. Mitchell, Moni Naor, Oscar Nierstrasz, C. Pandu Rangan, Bernhard Steffen, Madhu Sudan, Demetri Terzopoulos, Doug Tygar, Moshe Y. Vardi, Gerhard Weikum, Camille Salinesi, Moira C. Norrie, and Oscar Pastor, editors, *Advanced Information Systems Engineering*, volume 7908, pages 225–240. Springer Berlin Heidelberg, Berlin, Heidelberg, 2013.

[26] Corinna Cortes, Patrick Haffner, and Mehryar Mohri. Rational kernels: Theory and algorithms. *Journal of Machine Learning Research*, 5(Aug):1035–1062, 2004.

[27] G Cybenko. Approximation by superpositions of a sigmoidal function. *Mathematics of Control, Signals, and Systems*, pages 202–214, 1989.

[28] C. Danielski, T. Kacprzak, G. Tinetti, and P. Jagoda. Gaussian Process for star and planet characterisation. *arXiv:1304.6673 [astro-ph]*, April 2013.

[29] Thomas Desautels, Andreas Krause, and Joel W Burdick. Parallelizing Exploration-Exploitation Tradeoffs in Gaussian Process Bandit Optimization. page 51, December 2014.

[30] Tamara Djukic, Gunnar Flø"tterø"d, Hans Van Lint, and Serge Hoogendoorn. Efficient real time OD matrix estimation based on Principal Component Analysis. In *Intelligent Transportation Systems (ITSC), 2012 15th International IEEE Conference on*, pages 115–121. IEEE, 2012.

[31] David L. Donoho. High-dimensional data analysis: The curses and blessings of dimensionality. In *Ams Conference on Math Challenges of the 21st Century*, 2000.

[32] Nicolas Durrande, David Ginsbourger, Olivier Roustant, and Laurent Carraro. Additive covariance kernels for high-dimensional Gaussian process modeling, 2012.

[33] David Duvenaud. *Automatic model construction with Gaussian processes*. PhD thesis, University of Cambridge, 2014.

[34] Michael Florian, Michael Mahut, and Nicolas Tremblay. A hybrid optimization-mesoscopic simulation dynamic traffic assignment model. In *ITSC 2001. 2001 IEEE Intelligent Transportation Systems. Proceedings (Cat. No. 01TH8585)*, pages 118–121. IEEE, 2001.

[35] Gunnar Flötteröd, Michel Bierlaire, and Kai Nagel. Bayesian Demand Calibration for Dynamic Traffic Simulations. *Transportation Science*, 45(4):541–561, November 2011.

[36] Gunnar Flø"tterø"d. A general methodology and a free software for the calibration of DTA models. In *The Third International Symposium on Dynamic Traffic Assignment*, 2010.

[37] Peter I. Frazier. Bayesian Optimization. In *Recent Advances in Optimization and Modeling of Contemporary Problems*, INFORMS TutORials in Operations Research, pages 255–278. INFORMS, October 2018.

[38] Ken-Ichi Funahashi. On the approximate realization of continuous mappings by neural networks. *Neural Networks*, 2(3):183–192, January 1989.

[39] Alfredo Garcia, Stephen D. Patek, and Kaushik Sinha. A Decentralized Approach to Discrete Optimization via Simulation: Application to Network Flow. *Operations Research*, 55(4):717–732, August 2007.

[40] Andrew T. Glaws, Paul G. Constantine, and R. Dennis Cook. Inverse regression for ridge recovery: A data-driven approach for parameter reduction in computer experiments. *arXiv:1702.02227 [math]*, February 2017. arXiv: 1702.02227.

[41] Robert B. Gramacy and Herbert K. H. Lee. Adaptive Design and Analysis of Supercomputer Experiments. *Technometrics*, 51(2):130–145, May 2009.

[42] Robert B Gramacy and Herbert KH Lee. Cases for the nugget in modeling computer experiments. *Statistics and Computing*, 22(3):713–722, 2012.

[43] Robert B. Gramacy and Nicholas G. Polson. Particle Learning of Gaussian Process Models for Sequential Design and Optimization. *Journal of Computational and Graphical Statistics*, 20(1):102–118, January 2011.

[44] David K. Hale, Constantinos Antoniou, Mark Brackstone, Dimitra Michalaka, Ana T. Moreno, and Kavita Parikh. Optimization-based assisted calibration of traffic simulation models. *Transportation Research Part C: Emerging Technologies*, 55:100–115, June 2015.

[45] Martin L. Hazelton. Statistical inference for time varying origin–destination matrices. *Transportation Research Part B: Methodological*, 42(6):542–552, July 2008.

[46] J. C. Helton and F. J. Davis. Latin hypercube sampling and the propagation of uncertainty in analyses of complex systems. *Reliab. Eng. Syst. Saf.*, 2003.

[47] Dave Higdon, James Gattiker, Brian Williams, and Maria Rightley. Computer Model Calibration Using High-Dimensional Output. *Journal of the American Statistical Association*, 103(482):570–583, June 2008.

[48] Geoffrey E Hinton and Ruslan R Salakhutdinov. Using Deep Belief Nets to Learn Covariance Kernels for Gaussian Processes. In J. C. Platt, D. Koller, Y. Singer, and S. T. Roweis, editors, *Advances in Neural Information Processing Systems 20*, pages 1249–1256. Curran Associates, Inc., 2008.

[49] Kurt Hornik. Approximation capabilities of multilayer feedforward networks. *Neural Networks*, 4(2):251–257, January 1991.

[50] Donald R. Jones, Matthias Schonlau, and William J. Welch. Efficient global optimization of expensive black-box functions. *Journal of Global optimization*, 13(4):455–492, 1998.

[51] Kirthevasan Kandasamy, Jeff Schneider, and Barnabás Póczos. Bayesian Active Learning for Posterior Estimation. In *Proceedings of the 24th International Conference on Artificial Intelligence*, IJCAI'15, pages 3605–3611. AAAI Press, 2015. event-place: Buenos Aires, Argentina.

[52] Marc C. Kennedy and Anthony O'Hagan. Bayesian calibration of computer models. *Journal of the Royal Statistical Society: Series B (Statistical Methodology)*, 63(3):425–464, January 2001.

[53] Patrick Koch, Timothy Simpson, Janet Allen, and Farrokh Mistree. Statistical Approximations for Multidisciplinary Design Optimization: The Problem of Size. *Journal of Aircraft*, 36:275–286, January 1999.

[54] A. N. Kolmogorov. On the Approximation of Distributions of Sums of Independent Summands by Infinitely Divisible Distributions. *Sankhyā: The Indian Journal of Statistics, Series A* (1961-2002), 25(2):159–174, 1963. Publisher: Springer.

[55] Neil D. Lawrence. Gaussian process latent variable models for visualisation of high dimensional data. In *Advances in neural information processing systems*, pages 329–336, 2004.

[56] Jung Beom Lee and Kaan Ozbay. New calibration methodology for microscopic traffic simulation using enhanced simultaneous perturbation stochastic approximation approach. *Transportation Research Record*, (2124):233–240, 2009.

[57] M. J. Lighthill and G. B. Whitham. On kinematic waves II. A theory of traffic flow on long crowded roads. *Proceedings of the Royal Society of London. Series A. Mathematical and Physical Sciences*, 229(1178):317–345, May 1955.

[58] Xiaoyu Liu and Serge Guillas. Dimension Reduction for Gaussian Process Emulation: An Application to the Influence of Bathymetry on Tsunami Heights. *SIAM/ASA Journal on Uncertainty Quantification*, 5(1):787–812, January 2017.

[59] Chung-Cheng Lu, Xuesong Zhou, and Kuilin Zhang. Dynamic origin–destination demand flow estimation under congested traffic conditions. *Transportation Research Part C: Emerging Technologies*, 34:16–37, September 2013.

[60] Lu Lu, Yan Xu, Constantinos Antoniou, and Moshe Ben-Akiva. An enhanced SPSA algorithm for the calibration of Dynamic Traffic Assignment models. *Transportation Research Part C: Emerging Technologies*, 51:149–166, February 2015.

[61] T. Ma and B. Abdulhai. Genetic algorithm-based optimization approach and generic tool for calibrating traffic microscopic simulation parameters. *Intelligent Transportation Systems and Vehicle-highway Automation 2002: Highway Operations, Capacity, and Traffic Control*, (1800):6–15, 2002.

[62] Xingjun Ma, Yisen Wang, Michael E. Houle, Shuo Zhou, Sarah M. Erfani, Shu-Tao Xia, Sudanthi Wijewickrema, and James Bailey. Dimensionality-Driven Learning with Noisy Labels. *arXiv:1806.02612 [cs, stat]*, June 2018. arXiv: 1806.02612.

[63] Amandine Marrel, Bertrand Iooss, Michel Jullien, Béatrice Laurent, and Elena Volkova. Global sensitivity analysis for models with spatially dependent outputs. *Environmetrics*, 22(3):383–397, May 2011.

[64] M. D. McKay, R. J. Beckman, and W. J. Conover. A Comparison of Three Methods for Selecting Values of Input Variables in the Analysis of Output from a Computer Code. *Technometrics*, 21(2):239–245, 1979. Publisher: [Taylor & Francis, Ltd., American Statistical Association, American Society for Quality].

[65] M. Mesbah, M. Sarvi, and G. Currie. Optimization of Transit Priority in the Transportation Network Using a Genetic Algorithm. *IEEE Transactions on Intelligent Transportation Systems*, 12(3):908–919, September 2011.

[66] Mahmoud Mesbah, Majid Sarvi, Iraadj Ouveysi, and Graham Currie. Optimization of transit priority in the transportation network using a decomposition methodology. *Transportation Research Part C: Emerging Technologies*, 19(2):363 – 373, 2011.

[67] N Michelena and Panos Papalambros. Optimal Model-Based Partitioning of Powertrain System Design. June 2019.

[68] Jonas Mockus. *Bayesian Approach to Global Optimization: Theory and Applications*. Springer Science & Business Media, December 2012. Google-Books-ID: VuKoCAAAQBAJ.

[69] Jorge J Moré and Stefan M Wild. Benchmarking derivative-free optimization algorithms. *SIAM Journal on Optimization*, 20(1):172–191, 2009. Publisher: SIAM.

[70] Thomas Muehlenstaedt. Data-driven Kriging models based on FANOVA-decomposition, 2012.

[71] Kai Nagel and Gunnar Flötteröd. Agent-based traffic assignment: Going from trips to behavioural travelers. In *Travel Behaviour Research in an Evolving World—Selected papers from the 12th international conference on travel behaviour research*, pages 261–294. International Association for Travel Behaviour Research, 2012.

[72] Prasad A Naik and Chih-Ling Tsai. Constrained Inverse Regression for Incorporating Prior Information. *Journal of the American Statistical Association*, 100(469):204–211, March 2005.

[73] G. F. Newell. A simplified theory of kinematic waves in highway traffic, part II: Queueing at freeway bottlenecks. *Transportation Research Part B: Methodological*, 27(4):289–303, August 1993.

[74] Carolina Osorio and Krishna Kumar Selvam. Simulation-based optimization: achieving computational efficiency through the use of multiple simulators. *Transportation Science*, 51(2):395–411, 2017.

[75] Carl Edward Rasmussen and Christopher K. I. Williams. *Gaussian processes for machine learning*. Adaptive computation and machine learning. MIT Press, Cambridge, Mass, 2006. OCLC: ocm61285753.

[76] Paul I. Richards. Shock Waves on the Highway. *Operations Research*, February 1956.

[77] Philip A. Romero, Andreas Krause, and Frances H. Arnold. Navigating the protein fitness landscape with Gaussian processes. *Proceedings of the National Academy of Sciences*, 110(3):E193–E201, 2013.

[78] Roman Rosipal. Kernel Partial Least Squares for Nonlinear Regression and Discrimination. *Neural Network World*, (3):11, 2003.

[79] Elizabeth G. Ryan. *Contributions to Bayesian experimental design*. PhD thesis, Queensland University of Technology, 2014.

[80] Jerome Sacks, William J. Welch, Toby J. Mitchell, and Henry P Wynn. Design and Analysis of Computer Experiments. *Statistical Science*, 4(4):409–423, November 1989.

[81] Karim Saheb Ettabaa and Manel Ben Salem. Adaptive Progressive Band Selection for Dimensionality Reduction in Hyperspectral Images. *Journal of the Indian Society of Remote Sensing*, 46(2):157–167, February 2018.

[82] Andrea Saltelli, Stefano Tarantola, Francesca Campolongo, and Marco Ratto. *Sensitivity analysis in practice: a guide to assessing scientific models*, volume 1. Wiley Online Library, 2004.

[83] Alexandra M Schmidt, Kelly CM Gonçalves, and Patrícia L Velozo. Spatiotemporal models for skewed processes. *Environmetrics*, 28(6):e2411, 2017. Publisher: Wiley Online Library.

[84] Alexandra M. Schmidt, Peter Guttorp, and Anthony O'Hagan. Considering covariates in the covariance structure of spatial processes. *Environmetrics*, 22(4):487–500, June 2011.

[85] Laura Schultz and Vadim Sokolov. Bayesian Optimization for Transportation Simulators. *Procedia Computer Science*, 130:973–978, 2018.

[86] Di Sha, Kaan Ozbay, and Yue Ding. Applying bayesian optimization for calibration of transportation simulation models. *Transportation Research Record*, 2674(10):215–228, 2020.

[87] Amar Shah and Zoubin Ghahramani. Parallel Predictive Entropy Search for Batch Global Optimization of Expensive Objective Functions. *arXiv:1511.07130 [cs, stat]*, November 2015. arXiv: 1511.07130.

[88] Songqing Shan and G Gary Wang. Survey of modeling and optimization strategies to solve high-dimensional design problems with computationally-expensive black-box functions. *Structural and Multidisciplinary Optimization*, 41(2):219–241, 2010.

[89] Songqing Shan and G. Gary Wang. Survey of modeling and optimization strategies to solve high-dimensional design problems with computationally-expensive black-box functions. *Structural and Multidisciplinary Optimization*, 41(2):219–241, March 2010.

[90] Jeffrey A. Shorter, Precila C. Ip, and Herschel A. Rabitz. An Efficient Chemical Kinetics Solver Using High Dimensional Model Representation. *The Journal of Physical Chemistry A*, 103(36):7192–7198, September 1999.

[91] Jasper Snoek, Hugo Larochelle, and Ryan P. Adams. Practical bayesian optimization of machine learning algorithms. In *Advances in neural information processing systems*, pages 2951–2959, 2012.

[92] Jasper Snoek, Oren Rippel, Kevin Swersky, Ryan Kiros, Nadathur Satish, Narayanan Sundaram, Mostofa Patwary, Mr Prabhat, and Ryan Adams. Scalable bayesian optimization using deep neural networks. In *International conference on machine learning*, pages 2171–2180, 2015.

[93] Jasper Snoek, Kevin Swersky, Richard S. Zemel, and Ryan P. Adams. Input Warping for Bayesian Optimization of Non-Stationary Functions. In *ICML*, pages 1674–1682, 2014.

[94] A Srivastava, K Hacker, Kemper Lewis, and Timothy Simpson. A method for using legacy data for metamodel-based design of large-scale systems. *Structural and Multidisciplinary Optimization*, 28:146–155, September 2004.

[95] Jelka Stevanovic, Aleksandar Stevanovic, Peter T. Martin, and Thomas Bauer. Stochastic optimization of traffic control and transit priority settings in VISSIM. *Transportation Research Part C: Emerging Technologies*, 16(3):332 – 349, 2008.

[96] Matthew A. Taddy. Big Data: Factors, January 2018.

[97] Jian Tu and Donald Jones. Variable Screening in Metamodel Design by Cross-Validated Moving Least Squares Method. April 2003.

[98] Jialei Wang, Scott C. Clark, Eric Liu, and Peter I. Frazier. Parallel Bayesian Global Optimization of Expensive Functions. *arXiv:1602.05149 [math, stat]*, February 2016. arXiv: 1602.05149.

[99] Andrew Gordon Wilson, Zhiting Hu, Ruslan Salakhutdinov, and Eric P Xing. Deep kernel learning. In *Artificial Intelligence and Statistics*, pages 370–378, 2016.

[100] Jian Wu and Peter I. Frazier. The Parallel Knowledge Gradient Method for Batch Bayesian Optimization. *arXiv:1606.04414 [cs, stat]*, June 2016. arXiv: 1606.04414.

[101] Jing Xie, Peter I. Frazier, and Stephen E. Chick. Bayesian Optimization via Simulation with Pairwise Sampling and Correlated Prior Beliefs. *Operations Research*, 64(2):542–559, April 2016.

[102] Miao Yu and Wei (David) Fan. Calibration of microscopic traffic simulation models using metaheuristic algorithms. *International Journal of Transportation Science and Technology*, 6(1):63–77, June 2017.

[103] Chao Zhang, Carolina Osorio, and Gunnar Flötteröd. Efficient calibration techniques for large-scale traffic simulators. *Transportation Research Part B: Methodological*, 97:214–239, March 2017.

[104] Zhang Lei, Chang Gang-Len, Zhu Shanjiang, Xiong Chenfeng, Du Longyuan, Mollanejad Mostafa, Hopper Nathan, and Mahapatra Subrat. Integrating an Agent-Based Travel Behavior Model with Large-Scale Microscopic Traffic Simulation for Corridor-Level and Subarea Transportation Operations and Planning Applications. *Journal of Urban Planning and Development*, 139(2):94–103, June 2013.

[105] Xuesong Zhou. DYNAMIC ORIGIN-DESTINATION DEMAND ESTIMATION AND PREDICTION FOR OFF-LINE AND ON-LINE DYNAMIC TRAFFIC ASSIGNMENT OPERATION. August 2004. Accepted: 2004-08-27T05:36:30Z.

[106] Xuesong Zhou and Hani S. Mahmassani. A structural state space model for real-time traffic origin-destination demand estimation and prediction in a day-to-day learning framework. *Transportation Research Part B: Methodological*, 41(8):823–840, October 2007.

[107] Zheng Zhu, Chenfeng Xiong, Xiqun (Michael) Chen, and Lei Zhang. Calibrating supply parameters of large-scale DTA models with surrogate-based optimisation. *IET Intelligent Transport Systems*, April 2018.

[108] Byungkyu “Brian” Park, Ilsoo Yun, and Kyoungho Ahn. Stochastic optimization for sustainable traffic signal control. *International journal of sustainable transportation*, 3(4):263–284, 2009. Publisher: Taylor & Francis.